A Comparative Assessment of the NATO-GD and SFS2 Ship Airwakes and their Influence upon Helicopter Aerodynamic Loading

Nicholas Fernandez	Neale A Watson	Ieuan Owen	Mark D White
Ph.D. Student	Post-doctoral Researcher	Professor	Professor

University of Liverpool
Liverpool, UK

Abstract

The purpose of this study was to assess and compare the airwakes of two generic ship models, the NATO-GD and the SFS2, and their impact upon helicopter aerodynamic loading in operations over a ship's deck. Airwakes were computed using Delayed Detached Eddy Simulation, a time accurate CFD approach, for each ship model in a headwind and a Green 30 wind. The CFD airwakes were then integrated with a helicopter flight dynamics model, representative of an SH-60B Seahawk. The helicopter model was held stationary at a number of points along a lateral traverse profile over the flight deck of each ship, and the unsteady aerodynamic loads on the fixed-position helicopter were recorded and compared for the two ships. It was seen that the NATO-GD airwake created higher levels of turbulence and greater unsteady loads on the helicopter model than did the SFS2 airwake, implying greater workload for a pilot.

Introduction

Maritime helicopters are an essential aspect of modern naval operations, performing key tasks such as anti-submarine warfare, surveillance, troop-transfer, and supply replenishment. During launch and recovery operations, particularly in strong winds, shipboard helicopters are exposed to hazardous conditions which can elicit an extremely high workload for the pilot (Ref. 1). The unsteady turbulent air flow over a small landing deck that is moving due to sea conditions, and possibly a degraded visual environment, all contribute to the difficulty of the flying task over the deck. In conditions when pilot workload or helicopter performance limitations are reached, shipboard helicopter operations are restricted due to the potential risk to the helicopter and the ship, and to the crews. Such restrictions are defined by Ship-Helicopter Operating Limits (SHOLs), for each ship-helicopter combination and are determined by means of at-sea flight trials, which are costly and time-consuming. SHOLs are defined in terms of wind speed, wind direction and deck motion conditions for which it is determined to be safe for helicopters to land and take-off.

In support of shipboard helicopter operations, modelling and simulation (M&S) of the helicopter-ship dynamic interface (HSDI) can be used to predict how various factors influence helicopter handling qualities and pilot workload during launch and recovery. M&S can therefore be used as a tool to gain a deeper understanding of the HSDI and even reduce the costs associated with at-sea flight trials. Considerable international research efforts have been directed towards simulating the HSDI, including research conducted by the Flight Science and Technology research group at the University of Liverpool (UoL), which makes use of a six-degree-of-freedom flight simulator to provide pilots with motion and visual cues during simulated deck landings (Refs. 2-5). The M&S technical challenges that have been identified in flight simulation include accurately representing ship motion, ship airwake, and helicopter dynamics during piloted simulations (Ref. 6). While ship motion, helicopter dynamics and visual cues all affect pilot workload, the most significant contribution is the effect of the ship's airwake upon the aircraft. To aid in the understanding of how the air flow over the ship affects a helicopter and pilot, computational fluid dynamics (CFD) techniques are typically employed to generate time-accurate airwakes using methods that are now well-established (Ref. 7). The CFD-generated airwakes can then be integrated with a helicopter flight dynamics model and used to assess unsteady aerodynamic loads and aircraft handling qualities of shipboard helicopters when performing launch and recovery manoeuvres (e.g. Refs. 8,9).

To facilitate collaborative international research into the HSDI, the Simple Frigate Shapes (SFS and SFS2), simplified ship structural models, have been used extensively as common reference platforms to assess different CFD solutions (Refs. 10-17). The SFS2 model is intentionally simplified such that the shape can easily be replicated, and computational grids are simple to produce. However, the simplified model is increasingly unrepresentative of the more complex shape of modern frigates and destroyers. Over time, ship design has evolved to become stealthier with continuous slab-sided superstructures

which will influence the airwake over the deck and may affect aircraft performance and pilot workload. Consequently, the NATO Generic Destroyer (NATO-GD) ship model was proposed in Ref. 18. The NATO-GD is another notional ship model which provides a new common platform for the HSDI research community, where the geometry is more representative of modern destroyers than is the SFS2. Figure 1 illustrates both the SFS2 and the NATO-GD ship models where the progression of the design of the NATO-GD from the SFS2 can be seen. The sloping sides (tumblehome) of the NATO-GD are typical of a stealthy superstructure, which incorporates features such as a radar, exhaust stack, and mast as well as a larger hangar, all features which can commonly be seen in modern combat ships.

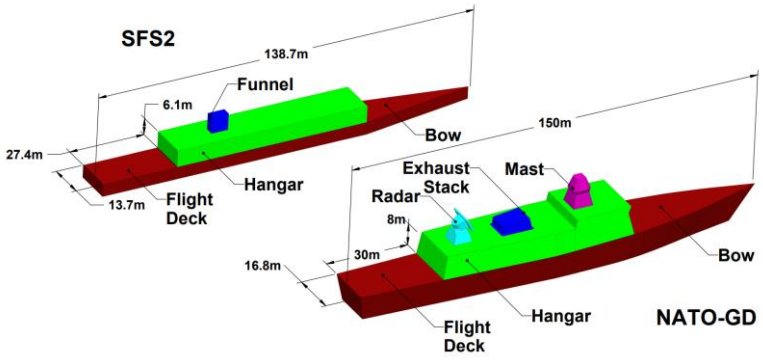

Figure 1. The Simple Frigate Shape 2 and NATO-Generic Destroyer ship geometry.

The aim of the study reported in this paper was to compare the aerodynamic characteristics of the SFS2 and NATO-GD ship models and to assess the impact of their airwakes upon helicopter aerodynamic loading during helicopter recovery operations. The airwakes were assessed by means of a CFD analysis, with a focus on the flow characteristics over the flight deck of each ship. The unsteady aerodynamic loading on a helicopter was evaluated by integrating the unsteady air velocities in the airwake with a helicopter flight dynamics model.

Method

Wind Conditions

Helicopter recovery to ships of the UK Royal Navy is conducted through a manoeuvre known as the forward-facing port-side approach, which is illustrated in Figure 2. The helicopter approaches along the port side of the ship, matching the ship's speed, before performing a lateral translation to a hover position over the landing spot, and then descending to touch down on the deck. This port-side manoeuvre is susceptible to strong oblique winds from the starboard side as the wind separates from the ship superstructure causing a turbulent air flow off the port side of the ship and in the path of the lateral translation. Therefore, two wind directions were selected for this study: a wind approaching from 30 degrees off the starboard, known as a Green 30 wind (G30), and a headwind i.e. a wind from the bow of the ship.

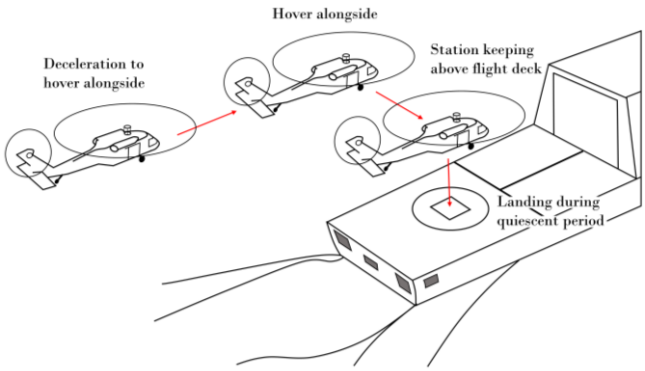

Figure 2. UK Royal Navy standard forward-facing port-side approach.

A steady atmospheric boundary layer (ABL) velocity profile was included as a boundary condition, as recommended by Ref. 19 where it was shown to create more realistic airwakes. The ABL was modelled using a power law velocity profile as used in Ref. 20, with a reference velocity of 20.58 m/s (40 knots) at a reference anemometer height for each ship, and a

power law exponent of 0.104 as suggested in Ref. 21. The reference anemometer height for each ship was taken to be at the height of the hangar: 17.25 m above sea level for the NATO-GD, and 10.67 m above sea level for the SFS2. The ABL profile is illustrated in Figure 3, where the normalised total velocity, V/V_{ref}, has been plotted against the normalised height above sea-level, z/z_{ref}. A side-view of the NATO-GD is also included in Figure 3.

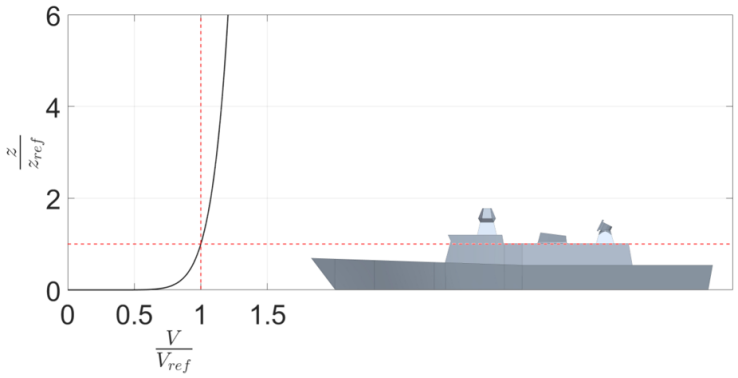

Figure 3. ABL velocity profile for inlet boundary condition.

CFD Approach

A time-accurate CFD approach, Delayed-Detached Eddy Simulation, was employed to calculate the unsteady turbulent air flow over each full-scale ship model; a variation of the Detached Eddy Simulation method originally recommended by Ref. 18. This method has since been utilized in subsequent CFD studies and has been validated against experimental data (Ref. 22). The method was implemented in the commercial CFD solver ANSYS Fluent where the solution strategy consisted of an initial steady state RANS solution computed using the k-ω SST turbulence model, a transient settling period of 15 s and a transient sampling period of 30 s, where a time step of 0.01 s was used in the transient calculations. An unstructured tetrahedral mesh was generated using ANSYS Meshing where a global cell sizing limit of 8 m was enforced and local sizing limits of 0.3 m placed at the ship surfaces. Cell growth was also restricted to 0.3 m in the space over the flight deck of each ship by using a density box; this ensured the turbulence was adequately resolved in the region where a helicopter would operate when recovering to the ship. Boundary layer meshing consisted of sixteen prism layers over the surface of the ships, resulting in a non-dimensional first layer height value in the range of 30-300. Figure 4 shows a section, over the flight deck of the NATO-GD, of an example computational mesh.

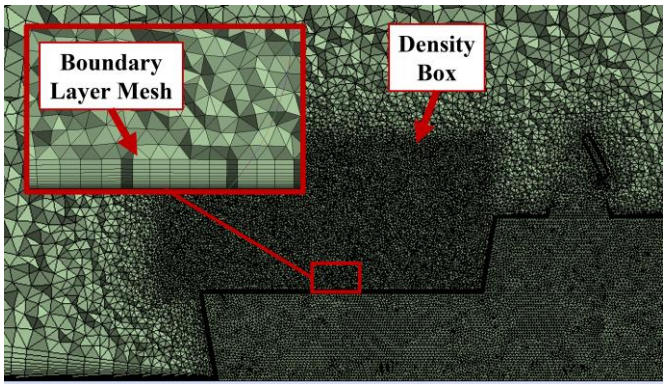

Figure 4. Computational mesh over the flight deck of the NATO-GD.

Calculation of Unsteady Helicopter Loads

An assessment of the unsteady aerodynamic loading on the helicopter was made using the Virtual AirDyn (VAD), a simulation tool developed at UoL (Ref. 8). The VAD is a software-based airwake dynamometer which calculates the unsteady forces and moments from a helicopter flight dynamics model held in a fixed position in a ship's airwake. To implement the VAD, the unsteady velocity components in the CFD-generated airwake were interpolated onto a cartesian grid with one-meter spacing, down-sampled to a rate of 25Hz, and then integrated with a helicopter flight dynamics model which had been developed previously using FLIGHTLAB (Ref. 23), a commercial software package which provides a multi-body modelling and simulation environment. The flight dynamics model was configured to be representative of a Sikorsky SH-60B Seahawk (Ref. 24). Once the ship airwake had been integrated with the helicopter flight dynamics model,

the helicopter controls were then trimmed in freestream conditions, away from the influence of the ship's airwake. When placed in the unsteady airwake, the three-dimensional unsteady airwake velocity components are applied to the helicopter flight dynamics model at 46 Airload Computation Points (ACPs) distributed over the structure of the helicopter, as illustrated in Figure 5. The ACPs are distributed as follows: 10 ACPs along each of the helicopter's four rotor blades, one ACP at the aerodynamic centre of the fuselage, four along the aerodynamic surfaces of the empennage, and one at the tail rotor hub. The resulting unsteady forces and moments acting on the helicopter are then calculated for the thirty-second period for which the airwakes had been calculated. Drag, side and thrust forces, and roll, pitch and yaw moments were calculated at the aircraft's centre-of-gravity (c.g.).

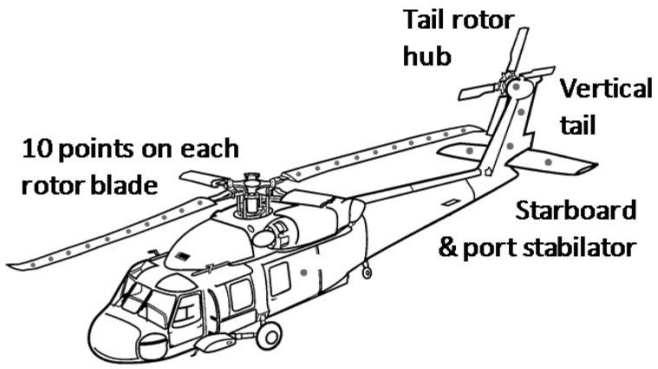

Figure 5. Airload Computation Points over the surface of the SH-60B Seahawk helicopter model (extracted from Ref. 8).

The metric that was extracted from the unsteady aerodynamic loads was the root-mean-square (RMS) of the load fluctuations. However, this metric, as defined by Ref. 8, is not defined as per the conventional definition of the term; instead, it is determined by deriving the power spectral density (PSD) from the force and moment time-histories and taking the square-root of the integral of the PSDs between the limits of 0.2 and 2Hz, hence quantifying only the fluctuations within a frequency range which is known to induce pilot workload (Ref. 25) and is, therefore, a more suitable metric of anticipated pilot workload.

Test Point Locations

The VAD technique was applied at a series of locations along a horizontal line representative of the lateral traverse manoeuvre of the port-side landing approach, described earlier. The line of test points (illustrated, for example, in Figure 7 and Figure 10), extends from one ship beam-width off the port-side edge of the flight deck to the starboard edge, spaced apart at one-quarter beam width increments. The beam width, in this instance, was taken to be the width of the flight deck at its longitudinal mid-point where the traverse spots were located. The c.g. of the helicopter was positioned at each of these locations at hangar height placing the pilot's eyeline at approximately hangar height, which is typical for recovery operations as the pilot can utilize the top edge of the hangar for visual cueing.

Results and Discussion

Ship Aerodynamics – CFD Analysis

The first airwake to be computed was for a headwind with a reference velocity of 20.58 m/s (40 knots). Figure 6 shows the headwind case as contour plots of the mean total velocity on a vertical longitudinal plane on the centreline of each ship, overlaid with two-dimensional streamlines, where the airwake of the NATO-GD is shown in Figure 6a and the airwake of the SFS2 shown in Figure 6b, a format which is consistent throughout all subsequent figures of the ships' airwakes in this discussion. In each airwake it can clearly be seen where there are reductions in air velocity compared with the freestream in the near vicinity and downstream of each ship. The decreased air velocities of the airwakes can be seen to approximately span the height of the superstructures; above this height the air velocity is the freestream value.

Several recirculation zones can be identified for both ships, such as in the lee of the hangar face, the stern of the ship, and other features on the superstructure, caused by flow separations that occur where there are sharp angles or sudden changes in direction in the superstructure geometries. The most significant recirculation zone concerning helicopter operations is in the lee of the hangar over the flight deck, where the air flow separates as it comes over the top and side surfaces of the

hangar, and then reattaches approximately half-way along the flight deck. Due to the bulkier superstructure of the NATO-GD, its recirculation regions are much larger, and the reduction in velocity above the flight deck occurs over a much greater height, potentially providing greater shelter for a helicopter from the oncoming wind when in the lee of the hangar. The resultant downdraft in this recirculation region over the deck of the NATO-GD has a much steeper gradient compared with the SFS2, which will have implications for the amount of thrust required for a helicopter operating in this region.

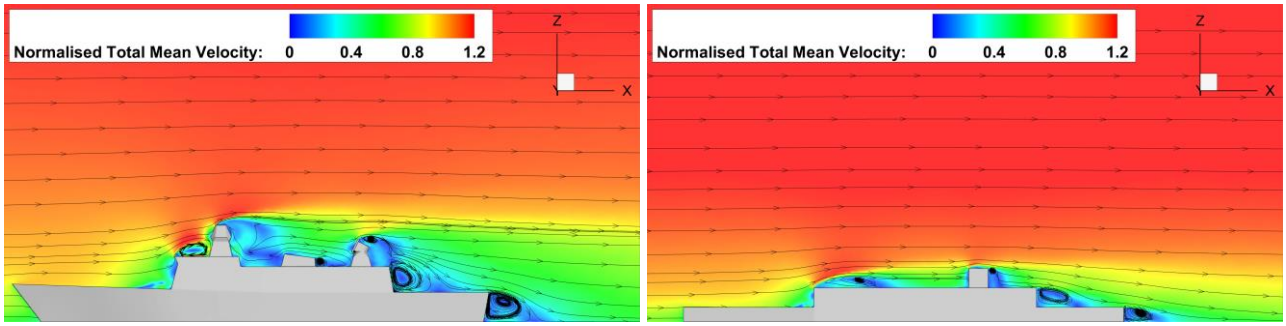

(a) **(b)**

Figure 6. Contour plots of normalised total mean velocity in vertical longitudinal planes located at the ships' centrelines for a headwind.

Figure 7 shows the mean total velocity in a vertical transverse plane at the longitudinal mid-point of the landing decks. The line of test points for the VAD analysis is also shown. The ABL velocity profile can be observed off either side of the ship in the freestream regions. The ABL velocity profile is seen to be different for each ship model; a greater velocity gradient is seen for the SFS2 than for the NATO-GD. This difference in the velocity profiles is due to the method used to apply the ABL; the reference height for the ABL velocity profile, which was placed at hangar height for each ship, is greater for the NATO-GD than the SFS2 due to its greater height, resulting in a higher velocity gradient above the sea surface. However, by applying the ABL in this way, the freestream velocity at the ship's hangar heights, and hence at the height of the helicopter's c.g. in the VAD analysis, is kept the same when making comparisons between the airwakes of each ship. It can be seen in Figure 7 that because of the larger hangar and superstructure features of the NATO-GD, the low velocity region is much broader than for the SFS2, hence providing further shelter from oncoming winds. The line of VAD test points is seen to move from the freestream velocity regions off the port side of the ship, through the effects of the ships' airwakes, over to the starboard edge of the ships' decks.

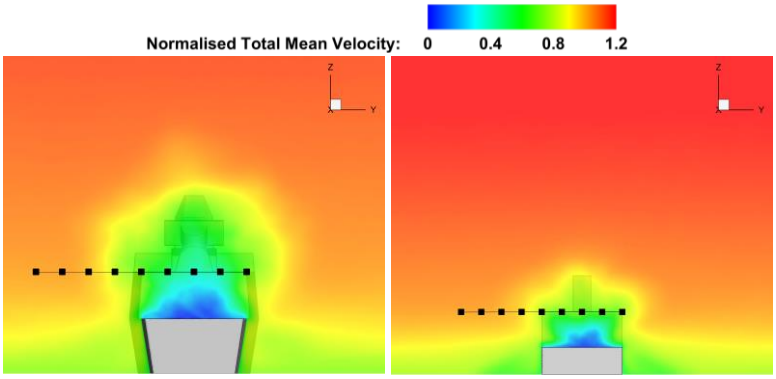

(a) **(b)**

Figure 7. Contour plots of normalised total mean velocity in transverse planes located at the deck mid-point for a headwind.

Figure 8 shows the turbulence intensity of the airwakes for each ship model in a vertical longitudinal plane along their centrelines (the black dot over each deck is a side -view of the line of VAD test points). The scale of the legend in these contour plots, and all subsequent plots of turbulence intensity, has been limited to a maximum of 25% to provide an optimal visual comparison between the ships' airwakes and to retain definition of the contour plots in the regions of interest above the ships' flight decks. However, in some instances the turbulence intensity does marginally exceed 25%, and these regions with the greatest turbulence intensities (i.e. 25% and above) are shown in red. The superstructure features, such as the mast,

radar and exhaust stack of the NATO-GD, and the funnel of the SFS2, are the sources of the most significant turbulence in the airwake. The turbulence intensity in the lee of the NATO-GD radar reaches up to 26%, while the comparable maximum turbulence intensity in the airwake of the SFS2 is lower and does not exceed about 20%. The lower turbulence intensities in the flight deck regions of each ship model can be seen to be in the range 10-15%. At the hover location over the landing spot, the turbulence generated by the funnel of the SFS2 has dissipated significantly, suggesting that the funnel of the SFS2 would not have a significant impact upon helicopter handling in this region where any turbulence would interact with the helicopter's rotor. However, the region directly above the flight deck of the SFS2, in the lee of the hangar, there is a region of greater turbulence when compared with the NATO-GD which would interact more so with the fuselage than the rotor. For the NATO-GD, the higher levels of turbulence created by the flow over the radar are sustained over the flight deck and a helicopter's rotor, when in hover over the deck, would be at least partially immersed in this more turbulent air.

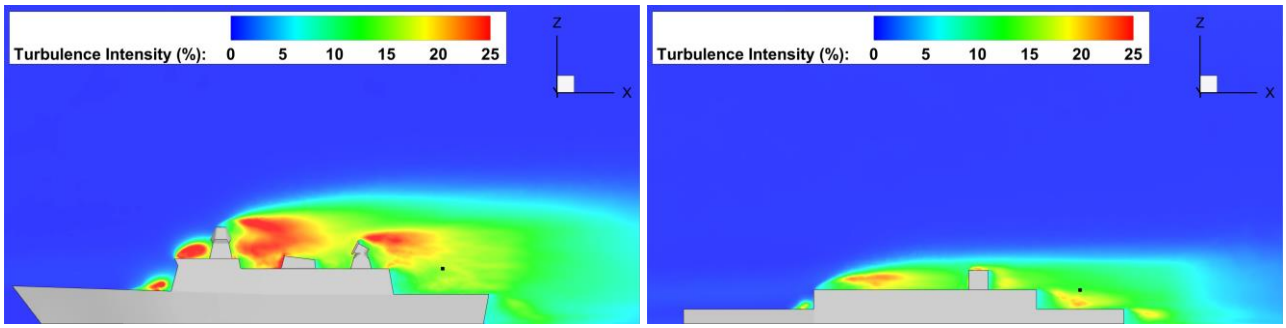

(a) **(b)**

Figure 8. Contour plots of turbulence intensity over vertical longitudinal planes located along the ships' centrelines for a headwind.

Figure 9 shows contour plots of turbulence intensity in a transverse plane located at the longitudinal mid-point of the deck of each ship model. Due to the larger superstructure of the NATO-GD, the region where turbulence is present in the airwake is much broader and taller than it is for the SFS2, and hence would expose a helicopter to air disturbances for a more significant duration during a landing. Whilst the turbulence in this region that is created by the superstructure features has somewhat dissipated by the deck mid-point, there are still levels of turbulence of up to 20-25% present over deck for both ships and which are predominantly generated by the hangar edges. The turbulence created by the SFS2 funnel has completely dissipated by the deck mid-point, and the turbulence that remains in this region is due solely to the hangar, whilst for the NATO-GD the radar causes an increase in turbulence intensity over deck, particularly where the helicopter's main rotor would be positioned. Directly over the deck of the SFS2, in the lee of the hangar, it can again be seen that the turbulence intensity is greater than that of the NATO-GD over the central portions of this region, whilst for the NATO-GD, greater turbulence intensity is observed over the deck's port and starboard edges.

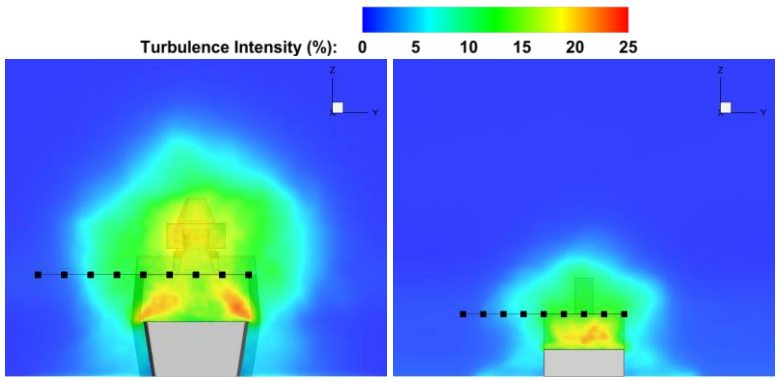

(a) **(b)**

Figure 9. Contour plots of turbulence intensity over transverse planes located at deck mid-point for a headwind.

The second wind condition that was assessed was a G30 wind, again with a reference velocity of 20.58 m/s (40 knots). As described earlier, this wind direction can be a challenge for helicopter pilots performing the standard UK naval port-side

approach as the turbulent air impacts the helicopter's approach path, as can be seen by the line of test points in Figure 10. In Figure 10 the G30 airwake is shown as contour plots of mean velocity overlaid with two-dimensional streamlines in horizontal planes located at hangar height for each ship model (i.e. 8m above flight deck for NATO-GD, and 6m for SFS2). Recirculation zones can be seen over the flight deck of each ship due to a flow separation that occurs on the starboard edge of the hangar. The recirculation zone of the NATO-GD is again larger than the SFS2; both images show the streamlines coming together, depicting the shear layers that separate the recirculation zones from the faster moving free stream.

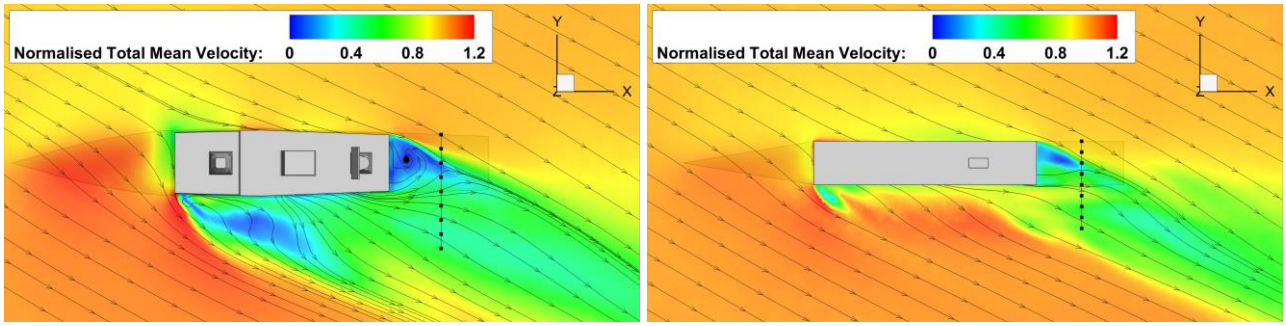

(a) **(b)**

Figure 10. Contour plots of normalised total mean velocity over horizontal planes located at hangar height for a G30 wind.

Figure 11 shows contour plots of mean velocity overlaid with two-dimensional streamlines in a transverse plane located at the decks' longitudinal mid-points. Large recirculation zones that extend to approximately two beam-widths off the port-side edge of each ship model can be observed as the oblique air flow separates from the top edges of the superstructure. The recirculation zones in this plane result in a more significant vertical velocity contribution and is therefore likely to have significant implications for the helicopter's aerodynamic thrust loading as it moves through the recirculating air. The downdraft of the airwake is less significant over the flight deck when compared with the headwind case, while over the starboard edge of the flight deck of each ship there is slight updraft as the air flows up and over the flight deck.

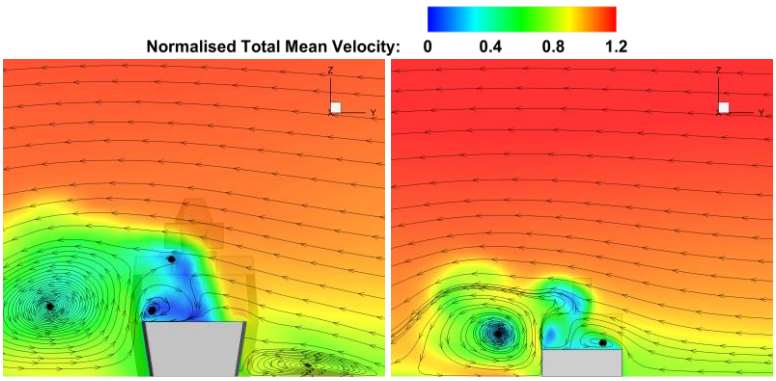

(a) **(b)**

Figure 11. Contour plots of normalised total mean velocity in transverse planes located at the deck mid-point for a G30 wind.

Figure 12 shows contours of turbulence intensity over a horizontal plane located at hangar height for each ship (i.e. at 8m and 6m respectively). The circles represent the areas occupied by the rotor disks for the two outermost positions of the traverse profile, along with the hover position over the deck spot. There are again higher levels of turbulence over the deck of each ship with the NATO-GD creating regions of turbulence intensity of up to 27%, compared with regions of 20-25% for the SFS2. When over the landing spot, for the NATO-GD most of the rotor disk is now immersed in turbulent air, whereas for the SFS2 the rotor disk is partially in clean air and partially immersed in the turbulent air. Off the port side of the landing deck, a higher turbulence intensity is created by the superstructure of the NATO-GD than for the SFS2, and there are greater contributions to the turbulence intensity from the forward sections of the superstructure of the NATO-GD than for the SFS2 due to the lack of features on the front half of its superstructure.

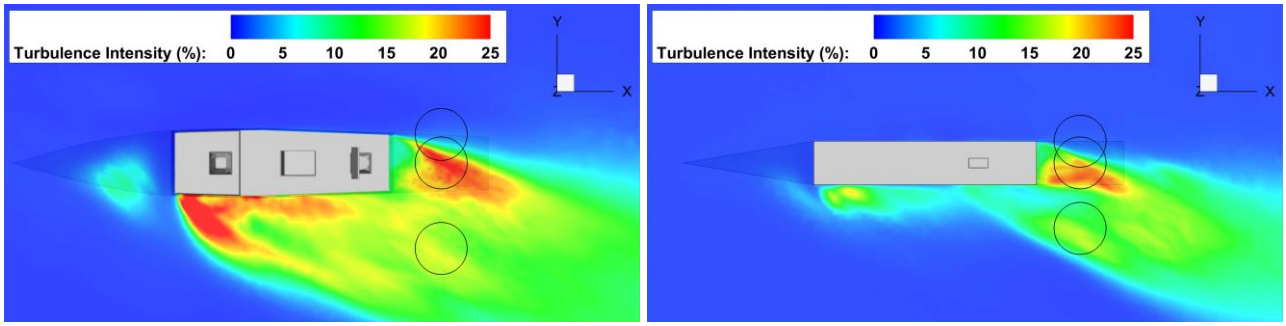

(a) **(b)**

Figure 12. Contour plots of turbulence intensity over horizontal planes located at hangar height for a G30 wind.

Figure 13 shows contour plots of turbulence intensity over a transverse plane located at the deck's longitudinal mid-point for each ship; the helicopter c.g. locations have again been shown. When compared with a headwind, in the G30 wind the superstructure features have a reduced impact upon the turbulence intensity over deck where the turbulence is created by the air flow separating from the windward vertical edges of the hangar, as well as from the deck edges. The turbulence is sustained as the flow reaches the landing spot at the centre of the deck, which was not the case for headwinds. The turbulent air covers the entirety of the helicopter's traverse across the deck from the port side for both ships; hence, the helicopter would be completely immersed in the turbulent air on the port-side of the ship, and the airwake of the NATO-GD is again much broader and taller than that of the SFS2. When compared with Figure 9, Figure 13 shows that there is not only an increase of up to 10% in turbulence intensity above that in the headwind case but that these high levels of turbulence are distributed over a much greater area, both of which will have consequences for the unsteady loads imposed on the helicopter translating across the deck.

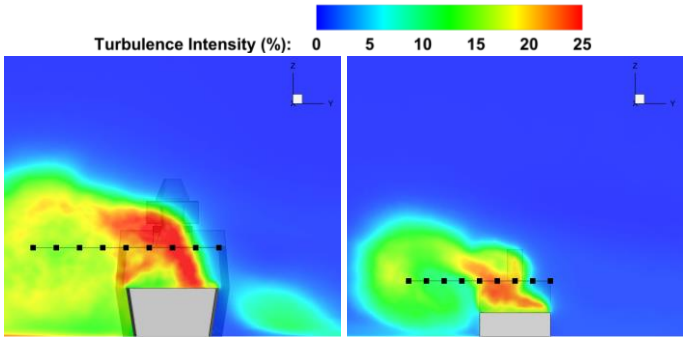

(a) **(b)**

Figure 13. Contour plots of turbulence intensity over transverse planes located at deck mid-point for a G30 wind.

VAD Analysis

The previous section has discussed the differences between the airwakes for the two ships in a headwind and a G30 wind, along with some of the implications for helicopter operations in these winds. However, the interaction between a helicopter and a ship airwake is complex, and it is unwise to draw too many conclusions regarding the possible effect of the airwake on the helicopter from the velocity field alone. The role of the VAD is to combine the unsteady velocities of the airwake with a flight dynamics model of the helicopter to quantify the integrated unsteady aerodynamic loads imposed onto the aircraft. The RMS of the load fluctuations that act upon a helicopter, within the frequency range 0.2 to 2Hz, are an indicative metric of pilot workload; larger fluctuations in helicopter aerodynamic loading can be expected to correlate with an increased pilot workload (Ref. 9). As a simplistic representation, high RMS load fluctuations in thrust would require a greater pilot workload in the collective pitch control, increased pitch and roll RMS load fluctuations would require greater workload in the cyclic control, and increased yaw RMS load fluctuations would require greater workload in the anti-torque pedal control. In reality, a coupling exists between the various controls and the six load components, but for this analysis the simplistic representation is sufficient as it identifies the overall effect of the unsteady airwake in each axis.

The RMS of the load fluctuations for the headwind case are presented in Figure 14, where each load component is plotted against the normalised helicopter c.g. lateral location relative to the ship's centreline, y/B, where B denotes the ship's beam width. In Figure 14, it is seen that not all load fluctuations are symmetric about the centrelines (y/B = 0). This asymmetry is due to the different effects on the advancing and retreating rotor blades; for example, in headwinds the streamwise component of the air velocity experienced by an advancing rotor blade would be greater than that of a retreating rotor blade hence causing asymmetric aerodynamic loads in a symmetrical airwake.

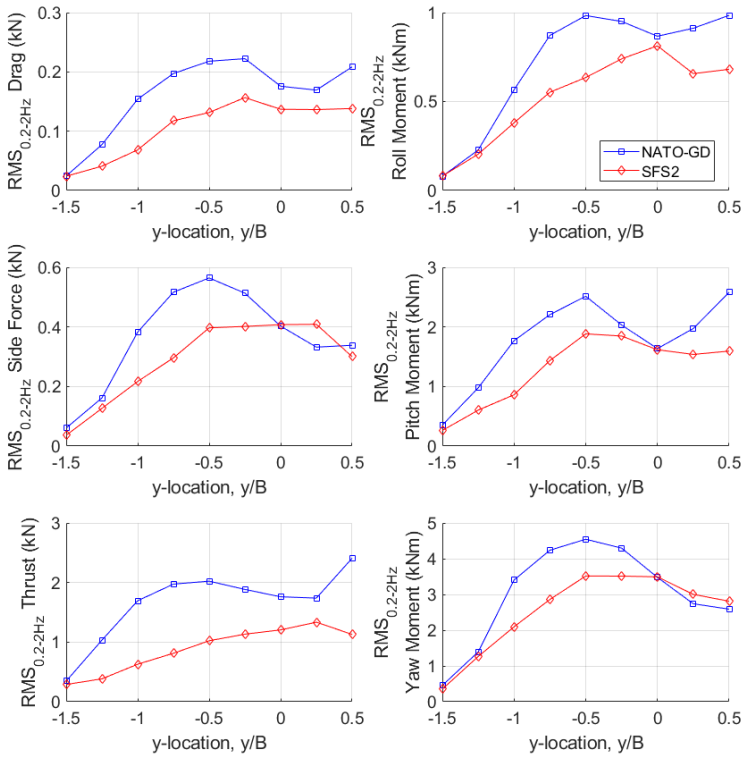

Figure 14. RMS of wind load fluctuations for a headwind.

For all axes, and both ships, there is an increase in load fluctuations when the helicopter is fully immersed in the airwake. When the helicopter is in the freestream regions (y/B = −1.5), the RMS load fluctuations begin to converge upon zero due to the turbulence intensity also approaching zero away from the influence of the airwake. It was seen in Figure 9 that the outer-most point on the port side, where the helicopter c.g. is located, is positioned outside of the airwake for both ships; however, the diameter of the rotor means that it will remain partially immersed in the airwake at this position. Whilst the helicopter's rotor is at least partially immersed in the ships' airwakes, the RMS load fluctuations will not reach zero.

At almost all helicopter positions, the RMS load fluctuations are greater for the NATO-GD than for the SFS2 indicating that a greater pilot workload would be required for recovery to the NATO-GD. In the case of the SFS2, the maximum RMS load fluctuations occur whilst over the deck spot (y/B = 0) where the turbulence intensity is greatest. However, in the case of the NATO-GD the maximum RMS load fluctuations occur approximately over the port-side edge of the flight deck (y/B = −0.5). Referring to Figure 9, this maximum in the RMS load fluctuations corresponds with an increase in the turbulence intensity in the regions over the edges of the flight deck and a local minimum in perturbations can be seen to exist directly over the landing spot. Whilst larger RMS load fluctuations can be seen for all axes for the NATO-GD, when compared with the SFS2, the axis in which the increase is greatest is thrust, suggesting that the collective pitch control would require the greatest input from the pilot. It can also be seen that for the NATO-GD the RMS thrust remains at a high level off the side of the ship until approximately one beam width to the port-side from deck centre (y/B = −1) where it then undergoes a sharp reduction. In comparison, the RMS thrust fluctuations for the SFS2 decrease at an almost constant rate from deck centre until the freestream. This comparison, although not as apparent as in the thrust loads, can also be observed for all other load axes and can be explained by the turbulence levels in the airwake; referring to Figure 9, a similar pattern can be observed where the turbulence intensity levels decrease further away from the deck spot. These patterns in the RMS load fluctuations suggest that a pilot may encounter a much more dynamic level of workload with abrupt changes in wind load perturbations as they traverse across the deck of the NATO-GD, compared with the SFS2.

The RMS load fluctuations for the G30 wind are presented in Figure 15. Like the headwinds case, the RMS load fluctuations for the NATO-GD are greater than the SFS2 across all six axes. For both ships, the RMS load fluctuations can be seen to follow similar trends across all axes, albeit with variations in magnitude. When compared with the RMS load fluctuations in a headwind, it can now be seen that the load fluctuations for the G30 wind begin to converge upon zero at the starboard side of the deck where the rotor is only partially immersed in the airwake (Figure 13). The greatest load fluctuations are present over the deck and to the port-side where the helicopter is immersed in the highest levels of turbulence. When the helicopter is positioned between the deck spot and the outer-most starboard point, the rotor is exposed to more clean air in the airwake of the SFS2 than for the NATO-GD, resulting in a sharper increase in RMS loads for the NATO-GD across all axes. These sharp increases are particularly prevalent in drag, side and yaw, load components which are more affected by the streamwise and lateral velocity components that are dominant in this region, as seen in Figure 10.

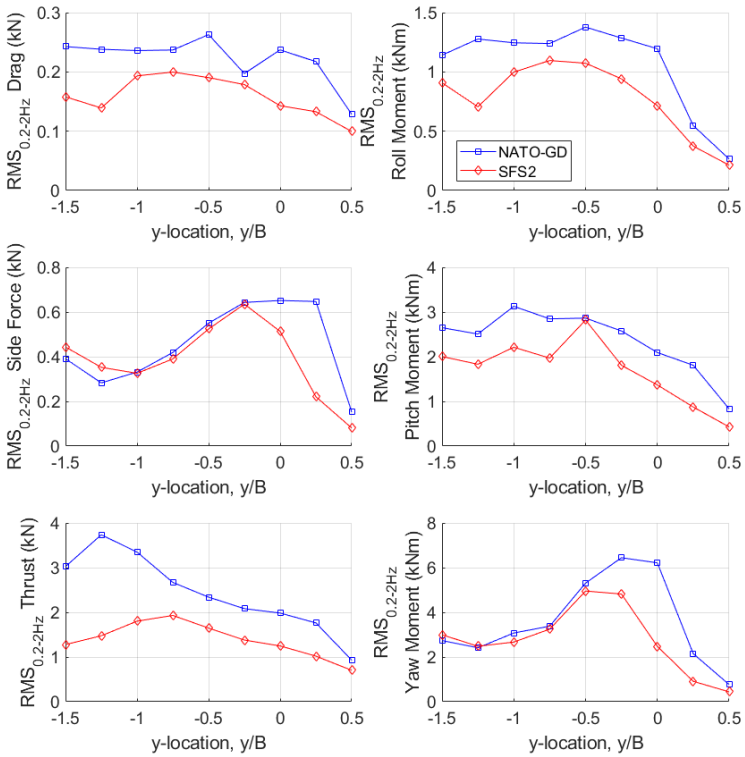

Figure 15. RMS of wind load fluctuations for a G30 wind.

There is a significant difference in RMS thrust between the two ships, with the NATO-GD experiencing fluctuations of approximately twice those of the SFS2 off the port side; the load fluctuations continue to rise to a maximum at −1.25 y/B in the case of the NATO-GD, whereas they peak at −0.75 y/B for the SFS2. These differences can be attributed to the greater levels of turbulence identified in this region in Figure 13; the rotor is exposed to greater turbulence intensity over a greater height and breadth for the NATO-GD and the turbulence is greater for the NATO-GD where there is a more significant vertical velocity component due to the taller superstructure.

CONCLUSIONS

An analysis of the aerodynamic characteristics of the NATO-GD and SFS2 notional ship models has been made for two wind conditions, headwind and G30, using time-accurate CFD. The normalised mean velocities and turbulence intensities in the flow over both ships have been compared, with a particular emphasis on how the airwakes might influence a helicopter operating to the flight deck of each ship. The unsteady wind loading on a helicopter representative of a Sikorsky SH-60B Seahawk was then calculated using the VAD, a software-based airwake dynamometer. The unsteady aerodynamic loads on the helicopter were determined at a series of locations in the airwakes along a line equivalent to a lateral traverse across the deck of each ship, a manoeuvre which is comparable to the UK Royal Navy port-side recovery.

The results of the analysis have highlighted how the geometry of the NATO-GD, which is more representative of modern destroyer class ships than is the SFS2, exacerbates the adverse effects that the ship's airwake has upon shipboard helicopter

operations. Flow structures which contribute to the unsteady loads on the helicopter have been identified in the airwakes of each ship. Greater RMS wind load fluctuations were obtained for the helicopter model in the airwakes of the NATO-GD than the SFS2 in both wind conditions and across all six load axes, implying a greater a pilot workload requirement. Whilst a harsher flying environment is undesirable for shipboard helicopter operations, the NATO-GD provides a more suitable platform than the SFS2 for HSDI research due to its more realistic representation of a modern combat ship.

The VAD analysis has demonstrated the more aggressive nature of the NATO-GD airwake, from the perspective of the helicopter, and how this implies greater workload for a pilot attempting to landing to the NATO-GD, compared with the SFS2. However, the potential increase in pilot workload cannot be quantified by the VAD and, therefore, a further study will be undertaken using a motion-base flight simulator to conduct piloted deck landings where the pilot will report workload using a recognized rating scale e.g., Deck Interface Pilot Effort Scale (Ref. 26) or the Bedford Workload rating scale (Ref. 27).

Acknowledgments

The authors would like to thank ANSYS Inc. for the continued support that they provide for the use of their products. The authors would also like to acknowledge and thank Dr. Christopher Dadswell for his support in the application of the simulation tools used in this work.

REFERENCES

1. Lumsden, R. B., Padfield, G. D., and Braby-Deighton, C. D., "Human Factors Challenges at the Helicopter-Ship Dynamic Interface," 1999 World Aviation Conference, San Francisco, CA, October 1999. DOI: 10.4271/1999-01-5607.
2. Owen, I., White, M. D., Padfield, G. D., and Hodge, S. J., "A virtual engineering approach to the ship-helicopter dynamic interface – a decade of modelling and simulation research at the University of Liverpool," *The Aeronautical Journal*, Vol. 121, (1246), 2017, pp. 1833-1857. DOI: 10.1017/aer.2017.102.
3. Roper, D. M., Owen, I., Padfield, G. D., Hodge, S. J., "Integrating CFD and piloted simulation to quantify ship-helicopter operating limits," *The Aeronautical Journal*, Vol. 110, (1109). 2006, pp. 419–428. DOI: 10.1017/S0001924000001329.
4. Watson, N. A., Owen, I., and White, M. D., "Piloted Flight Simulation of Helicopter Recovery to the Queen Elizabeth Class Aircraft Carrier," *Journal of Aircraft*, Vol. 57, (4). 2020, pp. 742-760. DOI: 10.2514/1.C035733.
5. White, M. D., Perfect, P., Padfield, G. D., Gubbels, A. W., and Berryman, A. C., "Acceptance testing and commissioning of a flight simulator for rotorcraft simulation fidelity research," *Proceedings of the Institution of Mechanical Engineers, Part G: Journal of Aerospace Engineering*, Vol. 227, (4), 2013, pp. 663-686. DOI: 10.1177/0954410012439816.
6. Healey, J. V., "Establishing a database for flight in the wakes of structures," *Journal of Aircraft*, Vol. 29, (4), 1992, pp. 559-564. DOI: 10.2514/3.46202.
7. Shukla, S., Sinha, S. S., Singh, S. N., "Ship-helo coupled airwake aerodynamics: A comprehensive review," *Progress in Aerospace Sciences*, Vol. 106, 2019, pp. 71-107. DOI: 10.1016/j.paerosci.2019.02.002.
8. Kääriä, C. H., Forrest, J. S., and Owen, I., "The virtual AirDyn: a simulation technique for evaluating the aerodynamic impact of ship superstructures on helicopter operations," *Aeronautical Journal*, Vol. 117, (1198), 2013, pp. 1233-1248. DOI: 10.1017/S0001924000008836.
9. Watson, N. A., Kelly, M. F., Owen, I., and White, M. D., "The Aerodynamic Effect of An Oblique Wind on Helicopter Recovery to The Queen Elizabeth Class Aircraft Carrier," Vertical Flight Society 75th Annual Forum & Technology Display, Philadelphia, PA, May 2019.
10. Bardera, R., Meseguer, J., "Flow in the near air wake of a modified frigate," *Proceedings of the Institution of Mechanical Engineers, Part G: Journal of Aerospace Engineering*, Vol. 229, (6), 2015, pp. 1003–1012. DOI: 10.1177/0954410014542449.
11. Hodge, S. J., Forrest, J. S., Padfield, G. D., Owen, I., "Simulating the environment at the helicopter-ship dynamic interface: research, development and application," *The Aeronautical Journal*, Vol. 116, (1185), 2012, pp. 1155–1184. DOI: 10.1017/S0001924000007545.

12. Hodge, S. J., Zan, S. J., Roper, D. M., Padfield, G. D., Owen, I., "Time-Accurate Ship Airwake and Unsteady Aerodynamic Loads Modeling for Maritime Helicopter Simulation," *Journal of the American Helicopter Society*, Vol. 54, (2), 2009. DOI: 10.4050/JAHS.54.022005.

13. Reddy, K. R., Toffoletto, R., Jones, K. R. W., "Numerical simulation of ship airwake," *Computers & Fluids*, Vol. 29, (4), 2000, pp. 451–465. DOI: 10.1016/S0045-7930(99)00033-X.

14. Syms, G. F., "Simulation of simplified-frigate airwakes using a lattice-Boltzmann method," *Journal of Wind Engineering and Industrial Aerodynamics*, Vol. 96, (6-7), 2008, pp. 1197–1206. DOI: 10.1016/j.jweia.2007.06.040.

15. Yuan, W., Wall, A., Lee, R., "Combined numerical and experimental simulations of unsteady ship airwakes," *Computers & Fluids*, Vol. 172, 2018, pp. 29–53. DOI: 10.1016/j.compfluid.2018.06.006.

16. Zan, S. J., "On aerodynamic modelling and simulation of the dynamic interface," *Journal of Aerospace Engineering*, Vol. 219, (5), 2005, pp. 393-410. DOI: 10.1243/095441005X30315.

17. Zhang, J., Minelli, G., Rao, A. N., Basara, B., Bensow, R., Krajnović, S., "Comparison of PANS and LES of the flow past a generic ship," *Ocean Engineering*, Vol. 165, 2018, pp. 221–236. DOI: 10.1016/j.oceaneng.2018.07.023.

18. Owen, I., Lee, R., Wall, A., and Fernandez, N., "The NATO generic destroyer – a shared geometry for collaborative research into modelling and simulation of shipboard helicopter launch and recovery," *Ocean Engineering*, Vol. 228, 2021. DOI: 10.1016/j.oceaneng.2020.108428.

19. Polsky, S. A., "CFD Prediction of Airwake Flowfields for Ships Experiencing Beam Winds," 21st AIAA Applied Aerodynamics Conference, Orlando, Florida, June 2003. DOI: 10.2514/6.2003-3657.

20. Forrest, J. S., and Owen, I., "An investigation of ship airwakes using Detached-Eddy Simulation," *Computers & Fluids*, Vol. 39, (4), 2010, pp. 656-673. DOI: 10.1016/j.compfluid.2009.11.002.

21. Counihan, J., "Adiabatic atmospheric boundary layers: A review and analysis of data from the period 1880–1972," *Atmospheric Environment (1967)*, Vol. 9, (10), 1975, pp. 871-905. DOI: 10.1016/0004-6981(75)90088-8.

22. Watson, N. A., Kelly, M. F., Owen, I., Hodge, S. J., and White, M. D., "Computational and experimental modelling study of the unsteady airflow over the aircraft carrier HMS Queen Elizabeth," *Ocean Engineering*, Vol. 172, 2019, pp. 562-574. DOI: 10.1016/j.oceaneng.2018.12.024.

23. Du Val, R. W., and He, C., "Validation of the FLIGHTLAB virtual engineering toolset," *The Aeronautical Journal*, Vol. 122, (1250), 2018, pp. 519-555. DOI: 10.1017/aer.2018.12.

24. Howlett, J. J., "UH-60A Black Hawk Engineering Simulation Program: Volume I – Mathematical Model", NASA-CR-166309, 1981.

25. McRuer, D. T., "Interdisciplinary interactions and dynamic systems integration," *International Journal of Control*, Vol. 59, (1), 1994, pp. 3-12. DOI: 10.1080/00207179408923067.

26. Carico, G. D., Fang, R., Finch, R. S., Geyer, W. P., Krijns, H. W., and Long, K., "Helicopter/Ship Qualification Testing," NATO RTO AGARDograph 300, Flight Test Techniques Series, Vol. 22, 2003.

27. Roscoe, A. H., and Ellis, G. A., "A subjective rating scale for assessing pilot workload in flight: A decade of practical use," Royal Aerospace Establishment TR 90019, 1990.